ACS OMEGA

http://pubs.acs.org/journal/acsodf

Article

Systematic Investigation of the Structure, Stability, and Spin Magnetic Moment of CrM_n Clusters (M = Cu, Ag, Au, and n = 2−20) by DFT Calculations

Nguyen Thi Mai,* Ngo Thi Lan,* Ngo Tuan Cuong,* Nguyen Minh Tam,* Son Tung Ngo,* Thu Thi Phung,* Nguyen Van Dang,* and Nguyen Thanh Tung*

Cite This: *ACS Omega* 2021, 6, 20341−20350

Read Online

ACCESS | Metrics & More | Article Recommendations | Supporting Information

ABSTRACT: Binary clusters of transition-metal and noble-metal elements have been gathering momentum for not only advanced fundamental understanding but also potential as elementary blocks of novel nanostructured materials. In this regard, the geometries, electronic structures, stability, and magnetic properties of Cr-doped Cu_n, Ag_n, and Au_n clusters (n = 2−20) have been systematically studied by means of density functional theory calculations. It is found that the structural evolutions of $CrCu_n$ and $CrAg_n$ clusters are identical. The icosahedral $CrCu_{12}$ and $CrAg_{12}$ are crucial sizes for doped copper and silver species. Small $CrAu_n$ clusters prefer the planar geometries, while the larger ones appear as on the way to establish the tetrahedral $CrAu_{19}$. Our results show that while each noble atom contributes one s valence electron to the cluster shell, the number of chromium delocalized electrons is strongly size-dependent. The localization and delocalization behavior of 3d orbitals of the chromium decide how they participate in metallic bonding, stabilize the cluster, and give rise to and eventually quench the spin magnetic moment. Moreover, molecular orbital analysis in combination with a qualitative interpretation using the phenomenological shell model is applied to reveal the complex interplay between geometric structure, electronic structure, and magnetic moment of clusters. The finding results are expected to provide greater insight into how a host material electronic structure influences the geometry, stability, and formation of spin magnetic moments in doped systems.

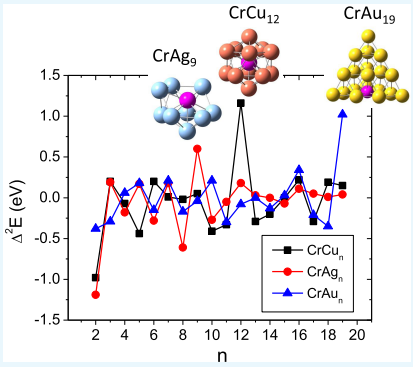

INTRODUCTION

Clusters of coinage metal atoms are fascinating pieces of matter.[1] Unlike their bulk counterparts, due to the large fraction of surface atoms and quantum size effects, the properties of coinage metal clusters evolve non-monotonically with their size.[2,3] While the size-dependent behavior of chemical and physical properties has been extensively investigated for pure species, many exciting challenges in doped coinage cluster systems remain to be explored.[4−8]

One of the emerging questions is to rationalize the interaction between localized impurity states and free electron gas, which allows us to detect the smallest limit from where complex phenomena as Friedel oscillations and the Kondo effect show up.[9−12] In this regard, the behavior of a coinage metal cluster doped with a transition-metal atom, where the electron cloud is well-controlled by the number of metal atoms in a cluster while the number of localized valence electrons is specified by the transition-metal atom, has been of significant interest.[13−17] For instance, the Fe and Co atoms in Ag_nCo^+ and Ag_nFe^+ were found to usually delocalize 4s electrons, but their all 4s and 3d valence electrons can be fully itinerant at specific sizes, i.e., $Ag_{10}Co^+$ and $Ag_{11}Fe^+$.[18] A similar electronic configuration was predicted for neutral $Ag_{10}Fe$, where the cluster magnetic moment is completely quenched due to the closed 18-electron shell structure.[19] A high relative dissociation energy as well as remarkably high abundance in the mass spectrum of $ScCu_{16}^+$ indicates its high stability in accordance with the predicted full occupation of the $1S^21P^61D^{10}$ shell configuration.[20−22] Although Cu, Ag, and Au are all noble metals, the hybridization between their s−d valence electrons can differently affect the properties of doped species. For example, the Au and Cu clusters were shown to dependently serve as either ferromagnetic or ferrimagnetic hosts to the Mn dopant's localized states.[23,24] The substitution of a V atom for a Cu atom in Cu clusters alters the odd−even oscillations of the host stability and magnetism in a different manner to that for a V atom in Au clusters.[25,26] The magnetic dopant thus interacts differently depending not only on the number of host valence electrons but also on the chemical properties of the host elements.[27]

Received: April 30, 2021
Accepted: July 15, 2021
Published: July 28, 2021

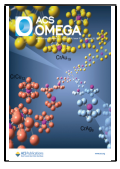

https://doi.org/10.1021/acsomega.1c02282
ACS Omega 2021, 6, 20341−20350

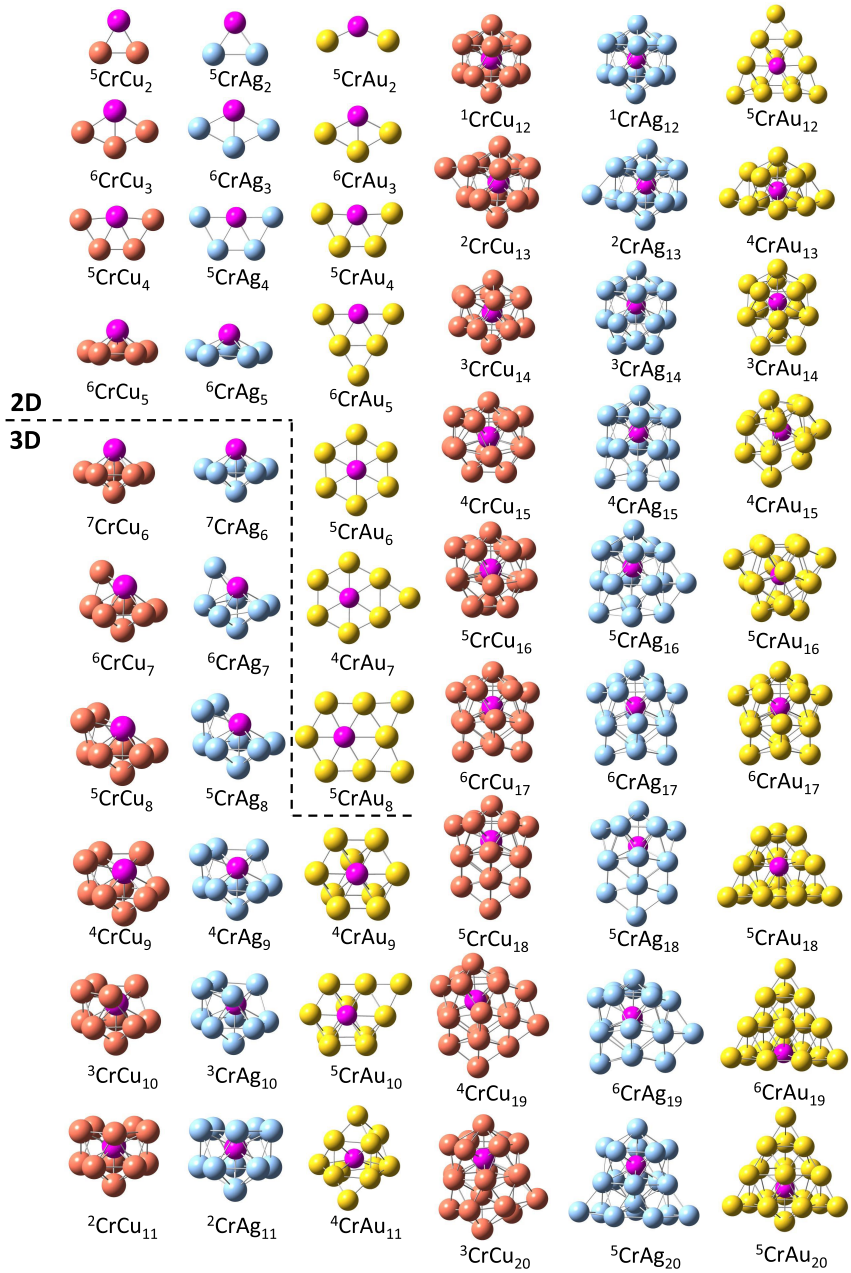

Figure 1. Most stable geometries and the corresponding spin multiplicities (superscript) of $CrCu_n$, $CrAg_n$, and $CrAu_n$ (n = 2−20).

Among transition-metal elements, Cr appears as an interesting dopant with six outermost electrons. Doping Cr in Cu_{12} was shown to form a Kondo-like system that enhances the cluster stability but quenches the magnetic moment simultaneously.[28] The size-dependent variation of the spin magnetic moment in Cr-doped Au clusters was observed in relation to the amount of hybridization between the impurity and the host density of states.[15−17] Unfortunately, a study that systematically addressed the size- and composition-dependent evolution of the structure, stability, and spin magnetic moments of Cr-doped coinage metal clusters has not been reported so far.

In this work, we study the lowest-energy structures, stability, and spin magnetic moments of CrM_n (M = Cu, Ag, and Au; n = 2−20) clusters as model systems that combine localized states, carried by the valence electrons of the impurity atom, with a tunable finite free electron gas formed by specific coinage metal stoichiometries. In particular, the most stable and other low-lying isomer structures of CrM_n are presented in Equilibrium Geometries and Growth Mechanism while Relative Stability describes the average binding energies, dissociation energies, and relative cluster stability. Their size-dependent multiplicities and electronic structures are examined and discussed in Size-Dependent Magnetic Moments and Electronic Structures. As the clusters grow, a two-dimensional (2D) to three-dimensional (3D) structural transition appearing at a specific size for each host species possibly alters the electronic structure and magnetic moment in different manners. These issues will be investigated, analyzed, and discussed in Interplay between Geometrical Structure, Electronic Structure, and Magnetic Moment. The conclusions are drawn in the final section.

https://doi.org/10.1021/acsomega.1c02282
ACS Omega 2021, 6, 20341−20350

COMPUTATIONAL METHOD

Geometry-unrestricted optimization was performed using density functional theory (DFT) with the BP86 functional in conjunction with the cc-pVTZ-pp basis set for Cu, Ag, and Au and the cc-pVTZ basic set for Cr as implemented in Gaussian 09 package.[29] The basis set cc-pVTZ-pp with an effective core potential already includes the relativistic effects that are crucial in the treatment of heavy elements such as Au. The search for the lowest-energy structures of CrM_n clusters was conducted using different approaches. First, a stochastic algorithm is applied to generate all possible structures.[30] In the second approach, the stable geometrical structures of CrM_{n-1} clusters were first optimized and then one more M atom was manually added to the low-lying isomers of the previous cluster size in all plausible positions to create input structures. Other energetically stable isomers of transition-metal-doped coinage metal clusters, which have been previously reported,[16,17,20−27] also served as reference input. We also considered all possible spin multiplicities for each geometry to ensure the robustness of the ground-state search. Each generated cluster was relaxed to the nearest local minimum. The stability of relaxed structures was investigated by calculating the harmonic vibrational frequencies and ones with no imaginary frequency were characterized as true minima. To achieve the computational accuracy without the additional increase in computing time, guessing structures were first optimized using the BP86 functional in conjunction with cc-pVDZ-pp for M atoms and cc-pVDZ for Cr one. Isomers with relative energies less than ∼50 kcal/mol were selected for recalculating single point energies at the same functional but combining with larger basis sets, cc-pVTZ-pp and cc-pVTZ, respectively. The electronic structure and magnetic property of CrM_n clusters were further explored using the molecular diagram and natural orbital analysis at the same level of theory. The convergence threshold parameters were set as follows: 2.0×10^{-5} Hartree for the energy and 5.0×10^{-3} Å for the displacement. It is worth mentioning that the BP86 functional has been proved to yield the most reliable results for different transition-metal-doped coinage metal systems.[16,17,20−22,28]

RESULTS AND DISCUSSION

Equilibrium Geometries and Growth Mechanism. An extensive search for global minima of $CrCu_n$, $CrAg_n$, and $CrAu_n$ with n equal to 2−20 is carried out and their corresponding ground-state structures are shown in Figure 1. Although a large number of possible structures and spin configurations are considered for each stoichiometry during the optimization process, only the lowest-energy isomers are discussed. Other low-lying energy isomers and their Cartesian coordinates are provided in the Supporting Information.[31]

The calculated results have shown that at small-sized CrM_n ($n \leq 5$ for M = Cu, Ag and $n \leq 8$ for M = Au) clusters prefer planar and quasi-planar structures. Species with larger sizes favor three-dimensional patterns. The Cr atom tends to occupy the most highly coordinated site and is encapsulated in the center of large-sized species. The structural evolutions of $CrCu_n$ and $CrAg_n$ clusters are identical. In particular, $CrCu_n$ and $CrAg_n$ clusters evolve to form a pentagonal pyramid at n equal to 5 and undergo a 2D−3D transition by establishing a pentagonal bipyramid at n equal to 6. For n equal to 7−12, the growth sequence tends to build up the second pentagonal pyramid, forming an icosahedral structure with the dopant at the center site. The clusters with n equal to 13 and 14 are produced by consecutively adding one and two Cu atoms to icosahedron with n equal to 12, respectively, resulting in a hexagonal antiprism structure. The growth of larger clusters can be approximately generalized by absorbing additional Cu atoms to the hexagonal antiprism core.[28] For doped gold clusters, the growth mechanism shows a different picture. $CrAu_n$ prefers planar at small sizes up to n equal to 8. A similar observation has been reported elsewhere.[32,33] The transition size of $CrAu_n$ clusters occurs at n equal to 9, where a layer-type structure is found. The layer-type motif is kept until n equal to 12. The tetrahedron $CrAu_{19}$ can be considered as a basic framework for $CrAu_n$ species with n equal to 13−19, as shown in Figure 1. $CrAu_{20}$ prefers an endohedral structure in which the Cr dopant is encapsulated in a distorted tetrahedral Au_{20}.

It should be mentioned that the 2D−3D transition appears at n equal to 7 for Cu_n and Ag_n and n equal to 13 for Au_n clusters.[34−36] The transition size of the Cr-doped clusters is smaller than that of the pure counterparts. Earlier studies also suggest that the transition-metal dopant can lower the transition size of coinage metal clusters. For instance, the first 3D configuration of VCu_n appears at n equal to 6 in form of a pentagonal bipyramid,[25] while the structural transition of $MnCu_n$ clusters was even found at n equal to 4 in the form of a distorted triangular bipyramid.[24] The 2D−3D transition for VAg_n is predicted to occur at n equal to 5, which is obviously smaller than that of the pure species.[26] VAu_n^+ cations experience a more complex structural transition. Their first 2D−3D transition is found at n equal to 7, followed by a final transition from a distorted planar VAu_8^+ back to 3D VAu_9^+.[27]

Our calculations show that the Cr dopant tends to occupy the highest coordinated position. This may be due to the fact that the Cr atom has a partially filled d shell. While the tetrahedron is still a basic framework for the growth process of $CrAu_n$ as well as their pure counterparts, the Cr dopant considerably influences the growth sequence of Cu and Ag clusters. The most stable isomers of pure Cu_n and Ag_n clusters undergo a transition from pentagonal bipyramid to double-layered structures for n equal to 6−12 and quasi-spherical and compact arrangements up to 18 atoms.[37] However, substituting one Cu or Ag atom by one Cr dopant, as presented in Figure 1, triggers a structural modification. In particular, for sizes n equal to 6−12, the growth sequence shows a build-up of an icosahedral structure from a pentagonal bipyramid. The growth of larger clusters is based on the icosahedral frame. This finding is in line with previous works, where the icosahedral structure was also found as the basic framework for VAg_n, VCu_n, VAg_n^+, and VAu_n^+.[25−27]

Relative Stability. To understand how the Cr dopant influences the stability of CrM_n clusters, we first examine the average binding energy per atom (E_b) of CrM_n and M_{n+1} clusters. The E_b values are determined by the following formulas

$$E_b(CrM_n) = \frac{1}{n+1}[(E(Cr) + nE(M)) - E(CrM_n)] \quad (1)$$

$$E_b(M_{n+1}) = \frac{1}{n+1}[(n+1)E(M) - E(M_{n+1})] \quad (2)$$

in which $E(Cr)$, $E(M)$, $E(CrM_n)$, and $E(M_{n+1})$ are the total energies of Cr, M, CrM_n, and M_{n+1}, respectively. In Figure 2a, the E_b values of CrM_n and M_{n+1} are presented as a function of cluster sizes for our comparison. Our calculated E_b values of Cu_{n+1}, Ag_{n+1}, and Au_{n+1} are in good agreement with the previous studies.[26,34,38−40] For $CrCu_n$ clusters, it is found that the average binding energy experiences two transitions. At small sizes ($n \leq$

https://doi.org/10.1021/acsomega.1c02282
ACS Omega 2021, 6, 20341−20350

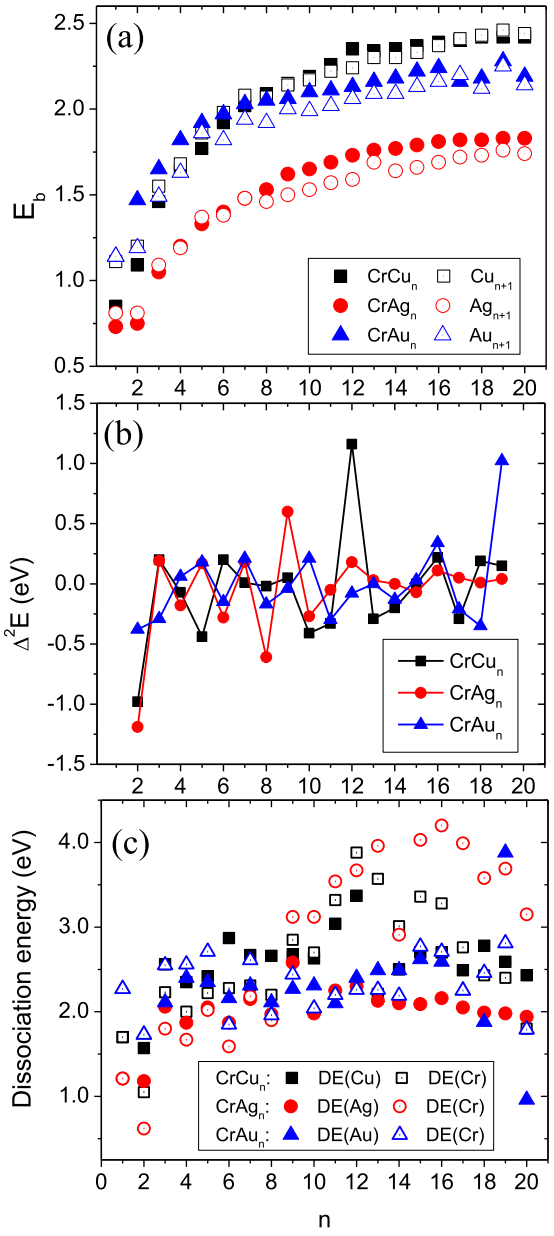

Figure 2. (a) Average binding energies (E_b) of M_{n+1} and CrM_n, (b) second-order differential energy (Δ_2E) of CrM_n, and (c) dissociation energies of CrM_n to evaporate one M or Cr atom.

7), E_b of $CrCu_n$ is smaller than that of Cu_{n+1}. The average binding energy of $CrCu_n$ is considerably higher than that of Cu_{n+1} at n equal to 8−16, especially for n ≥ 12. For larger-sized species, the difference between E_b of Cu_{n+1} and that of $CrCu_n$ is negligible. A similar trend is observed for $CrAg_n$, and their pure counterparts in which the transition for E_b of $CrAg_n$ also appears at n equal to 8. This can be linked to the fact that the most stable isomers of pure Cu_n and Ag_n clusters evolve from pentagonal bipyramid at n equal to 6 to double-layered structures, quasi-spherical, and compact arrangements up to 18 atoms.[37] Substituting a Cu or Ag atom by a Cr dopant, as presented in Figure 1, triggers a structural modification: the growth sequence of doped species shows a build-up of an icosahedral structure at n equal to 12, which is a central core for larger doped clusters as well. The average binding energy of $CrAu_n$ clusters is generally higher than that of Au_{n+1}, implying that doping Cr seems to stabilize Au clusters. A noticeable difference is observed for both $CrAu_{19}$ and Au_{20}, agreeing with the relatively high stability of the 20-atom pyramidal structures.[16,17]

The relative stability of CrM_n among neighboring sizes is analyzed using the second-order different energy (Δ_2E) as follows

$$\Delta_2E(CrM_n) = E(CrM_{n+1}) + E(CrM_{n-1}) - 2E(CrM_n) \quad (3)$$

The calculated values of Δ_2E as a function of the cluster size are plotted in Figure 2b. For $CrCu_n$ clusters, a distinct maximum is found at n equal to 12, in line with the well-known exceptionally high stability of $CrCu_{12}$ among other species.[28] Two other conspicuous peaks are recorded for $CrAg_9$ and $CrAu_{19}$, deducing that they are more stable than their neighbors. Although the $CrCu_2$ and $CrAg_2$ clusters have the smallest values of Δ_2E, the second-order energy differences of other species either stay nearly constant or less noticeable.

To further comment on the stable patterns observed above, the dissociation energies required for CrM_n clusters to evaporate a Cr atom and a M atom are respectively calculated as

$$DE(Cr) = E(M_n) + E(Cr) - E(CrM_n) \quad (4)$$

and

$$DE(M) = E(CrM_{n-1}) + E(M) - E(CrM_n) \quad (5)$$

Those energies are obtained by assuming the lowest-energy structures and spin states for the mother cluster and the fragments with an estimated error margin on thermodynamic parameters of about ±0.3 eV. The results are presented in Figure 2c. It is expected from the detailed balance theory that the evaporative rate constant depends strongly on the dissociation energy and the evaporation channel associated with the lowest dissociation energy is most favorable.[41,42] The dissociation of a Cr atom is the most fragile channel for $CrCu_n$ with $n \leq 8$. From then on, the separation of a Cu atom is energetically preferred until n is equal to 17. $CrCu_{18}$, $CrCu_{19}$, and $CrCu_{20}$ again favor the loss of a Cr atom. $CrCu_{12}$ icosahedron manifests its outstanding stability by requiring at least 3.37 eV to evaporate a Cu atom or 3.88 eV to release a Cr atom. With one more Cu atom, $CrCu_{13}$, however, is much unstable and needs only 2.21 eV to fragment into $CrCu_{12}$ and a Cu atom. This can be understood by the fact that $CrCu_{13}$ is composed of one additional Cu atom attached to the surface of a stable icosahedral $CrCu_{12}$ unit. $CrCu_2$ and $CrCu_4$ are also unstable species, which only require 1.05 and 2.00 eV to dissociate into Cu_2 and Cu_4 via the loss of a Cr atom, respectively. A transition at n equal to 8 is also observed in the fragmentation behavior of doped silver clusters. In particular, $CrAg_n$ clusters tend to evaporate a Cr atom for $n \leq 8$ and a Ag atom for n of 9. $CrAg_2$ and $CrAg_6$ are the most unstable stoichiometries, which require only 0.62 and 1.59 eV to dissociate into Ag_2 and Ag_6, respectively. The calculated DEs indicate that $CrAg_9$ is the most stable species among the doped silver ones. The minimum energy to break this cluster is 2.58 eV, even higher than that of the icosahedral $CrAg_{12}$ (2.30 eV). This result is also in accordance with the above analysis based on the second-order difference of energies. Unlike $CrCu_n$ and $CrAg_n$, the dissociation behavior of doped gold clusters is strongly size-dependent. The stability of $CrAu_{19}$ is most pronounced since it requires at least 2.81 and 3.88 eV to vaporize a Cr atom and a Au atom, respectively. Taking this into account, it is quite straightforward that $CrAu_{20}$ is the most fragile

https://doi.org/10.1021/acsomega.1c02282
ACS Omega 2021, 6, 20341−20350

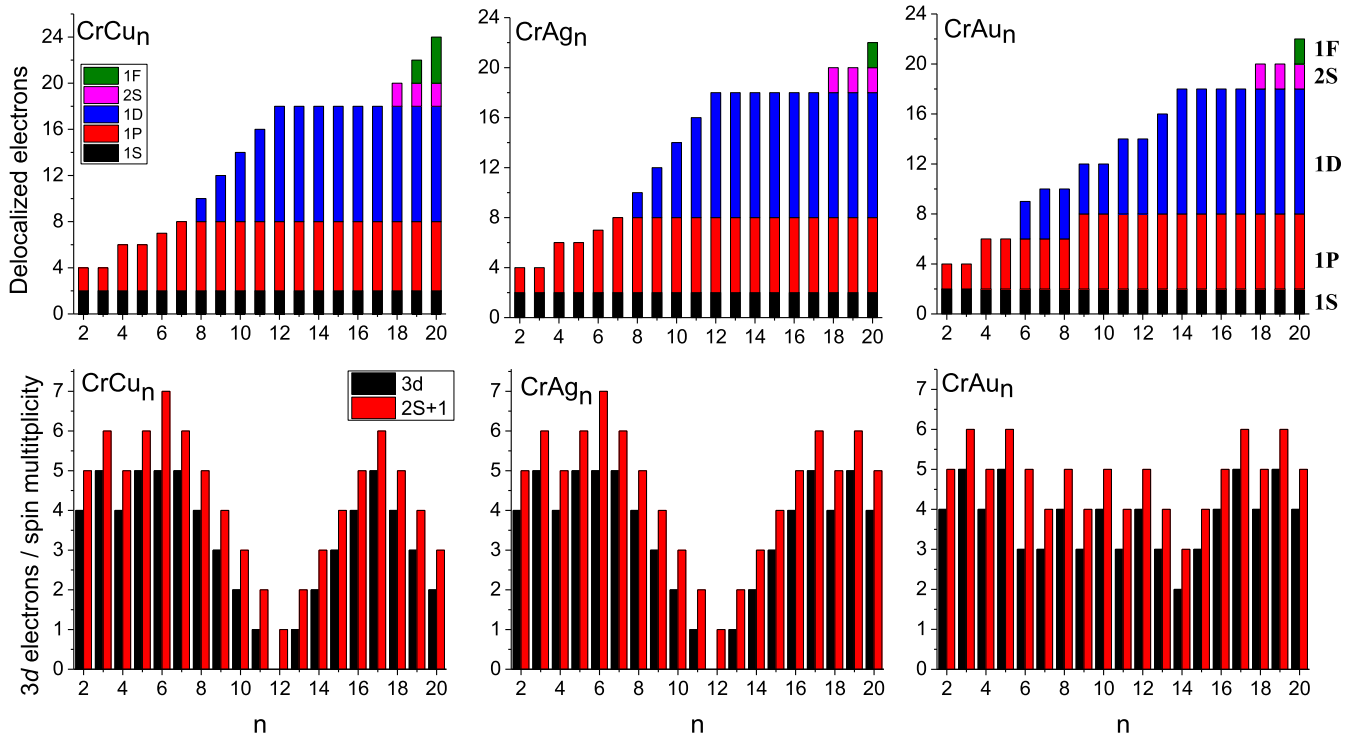

Figure 3. Electronic shell fillings, occupations of the localized 3d chromium orbitals, and spin multiplicities for $CrCu_n$, $CrAg_n$, and $CrAu_n$ (n = 2−20). The black, red, blue, pink, and green columns in the electronic shell filling diagrams represent the occupation of the 1S, 1P, 1D, 2S, and 1F shell, respectively.

one, requiring only 0.96 eV to break into the stable $CrAu_{19}$ and Au atom.

Size-Dependent Magnetic Moments and Electronic Structures. One of the most interesting features offered by transition-metal-doped noble-metal clusters is their non-monotonic size-dependent magnetic behavior. Typically, when a magnetic impurity like the Cr atom is introduced into the cluster of noble metals, the valence orbitals of the impurity can hybridize with the delocalized orbitals of the host to form localized and delocalized molecular orbitals. While each noble-metal atom generally donates one s itinerant electron, the delocalization of six valence electrons in $4s^13d^5$ of the Cr dopant depends on the electronic structure and the geometry of the cluster. Figure 3 illustrates the electronic shell filling and spin multiplicities of the clusters. Generally, the chromium atom possesses a $3d^54s^1$ configuration in these clusters. Clusters of $CrCu_n$ and $CrAg_n$ show a similar filling rule. In particular, the chromium atom contributes either one (s) or two (one s and one d) electrons to the cluster shell of the small $CrCu_n$ and $CrAg_n$ clusters until n is equal to 7, except for n equal to 6, to complete the subshell $1S^21P^6$, resulting in the multiplicity alternation between 5 and 6 (corresponding to magnetic moments of 4 and 5 μ_B), respectively. Both $CrCu_6$ and $CrAg_6$ exhibit a septet multiplicity (corresponding to a magnetic moment of 5 μ_B) due to their $1S^21P^43d^51P^1$ electron gas configuration. For n from 8 to 12, the Cr dopant gradually donates from two to all six electrons to fill the subshell 1D. For both $CrCu_{12}$ and $CrAg_{12}$, all six valence electrons of the chromium dopant delocalize to the electron gas of the cluster giving rise to a $1S^21P^61D^{10}$ closed-shell configuration and a quenched magnetic moment (singlet multiplicity). This shell-closure configuration is kept until n is equal to 17, while the spin multiplicity increases from singlet to sextet (0−6 μ_B) due to the decrease of the delocalized Cr electrons. Both $CrCu_{18}$ and $CrAg_{18}$ exhibit a configuration of $1S^21P^61D^{10}2S^2$, with one 4s and one 3d delocalized electrons from Cr atom, giving a magnetic moment of 4 μ_B (quintet multiplicity). From here, the 1F subshell starts to be filled from n equal to 19 in $CrCu_n$ and from n equal to 20 in $CrAg_n$ clusters, which correspondingly change their multiplicities: $CrCu_{19}$ and $CrCu_{20}$ have a quartet and triplet (3 and 2 μ_B), while $CrAg_{19}$ and $CrAg_{20}$ possess a sextet and a quintet (5 and 4 μ_B), respectively.

$CrAu_n$ clusters follow a different filling route. As the size increases, the cluster shells are gradually filled and the first shell closure is obtained at n equal to 14 with a configuration of $1S^21P^61D^{10}$. When n goes from 2 to 5, the multiplicity alternates between 5 and 6 like that of Cu and Ag counterparts. $CrAu_6$ also has a magnetic moment of 4 μ_B (quintet multiplicity) with three 3d localized electrons in the Cr atom and one unoccupied 2P electron in the molecular shell. The multiplicity alternation between 4 and 5 starts again when n goes from 7 to 13. The Cr atom donates three 3d and one 4s valence electrons to the electron gas of $CrAu_{14}$ to form the closed-shell $1S^21P^61D^{10}$ with a triplet spin state (2 μ_B). From n equal to 15, the electronic configuration and spin multiplicity of $CrAu_n$ are similar to those of $CrAg_n$. It should be noted that the 1D cluster orbitals are already occupied in $CrAu_6$, while they first appear in $CrCu_n$ and $CrAg_n$ at n equal to 8. This observed picture is in line with previous results for vanadium-doped noble-metal clusters.[27] It is also important that the filling of the 1D cluster orbitals is interrupted in the VAu_7^+ to form the $1S^21P^6$ shell closing with a preferred 3D geometry but not in the planar $CrAu_7$ with the $1S^21P^41D^4$ configuration. Unlike in doped copper and silver clusters, where the chromium 3d orbitals can fully participate in the cluster electron gas (at n equal to 12), this has not been observed for the $CrAu_{2-20}$ clusters. The 3d orbitals are spatially confined at the Cr impurity in the doped gold clusters and the

https://doi.org/10.1021/acsomega.1c02282
ACS Omega 2021, 6, 20341−20350

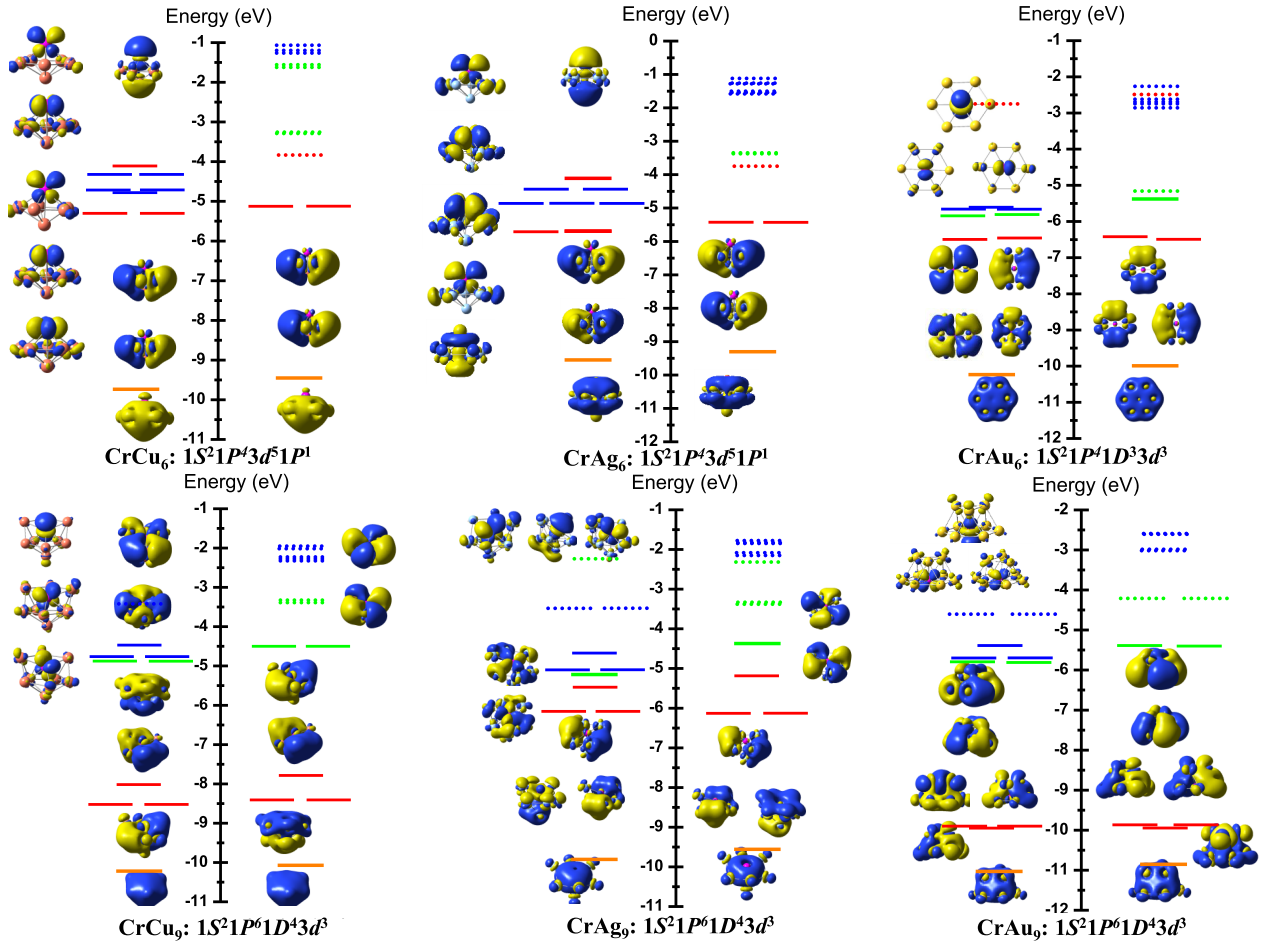

Figure 4. Molecular orbital diagrams for CrM_n (n = 6 and 9) with pictures of the delocalized orbitals and the localized 3d Cr orbitals. The orange, red, and green lines represent orbitals corresponding to the 1S, 1P, and 1D shells, respectively. The blue lines represent the localized 3d Cr orbitals. The filled lines stand for occupied orbitals while the dashed lines denote the unoccupied ones.

maximum number of delocalized 3d Cr electrons is three at n equal to 14.

Interplay between Geometrical Structure, Electronic Structure, and Magnetic Moment. To understand the evolution of the electronic structure as well as to gain insight into the magnetic behavior, we calculated the molecular orbital diagrams of the CrM_n clusters. The results for some specific species related to the 2D−3D transition and stability enhancement, for example, CrM_6, CrM_9, CrM_{12}, and CrM_{19}, are plotted in Figures 4 and 5. The molecular orbital diagrams for other clusters are provided in the Supporting Information.[31]

The transition from two- to three-dimensional structure at n equal to 6 is worthy of further discussions. Small $CrCu_n$ and $CrAg_n$ clusters up to n equal to 5 prefer planar geometries, resulting in electronic structures with a magic number of six: $1S^21P_x^23d^4$ (n = 2), $1S^21P_x^23d^5$ (n = 3), $1S^21P_x^21P_y^23d^4$ (n = 4), and $1S^21P_x^21P_y^23d^5$ (n = 5). Since six is a subshell closure for oblate deformations in the Clemenger−Nilsson model, the gap between $1P_x1P_y$ and $1P_z$ is relatively large. Either four or five localized 3d electrons in the Cr dopant are therefore responsible for the magnetic moment of the clusters. $CrCu_6$ and $CrAg_6$ prefer 3D structures. Several stable isomers are identified for $CrCu_6$ and $CrAg_6$, but the pentagonal bipyramid is the most stable one. This geometric transition lowers the energy level of the $1P_z$ orbital to be partially filled. As the 1D delocalized orbitals are still too high in energy, only one 4s valence electron of the Cr atom participates in the cluster shell, resulting in the electronic structure $1S^21P_x^21P_y^23d^51P_z^1$. The filled $1P_z^1$ and localized $3d^5$ in the majority channel are responsible for a spin magnetic moment of 6 μ_B. On the other hand, $CrAu_6$ has a high symmetric hexagonal structure with the dopant in the center of the cluster, causing an upshift of $1P_z$ level. Although $1S^2$, $1P_x^2$, and $1P_y^2$ orbitals are filled, only three localized 3d electrons are found in the Cr atom. The other 3d electrons are delocalized and participate in the cluster shells to form the 1D orbital, resulting in an electronic structure of $1S^21P_x^21P_y^21D^33d^3$ and a magnetic moment of 4 μ_B. It is obvious that the delocalization behavior of the dopant valence electrons, which reflect a major part of the cluster magnetic moment, depends on the electronic structure and the geometry of the cluster. This analysis of the molecular orbitals is in line with previous conclusions on VM_n clusters that the transition from two- to three-dimensional structures of CrM_n is rooted in the filling of the $1P_z$ cluster orbital, irrespective of the coin metal.

$CrCu_9$, $CrAg_9$, and $CrAu_9$ all prefer three-dimensional structures, resulting in the $1P_z$ orbital being completely occupied and 1D orbital eventually becoming filled. These clusters have the same electronic structures, $1S^21P^61D^43d^3$, and the same magnetic moment, 3 μ_B. In all three clusters, the Cr atom donates one 4s and two 3d electrons to participate in metallic bonding with the M atoms via a pool of 12 itinerant electrons. Three localized electrons remaining in the 3d orbital cause a

https://doi.org/10.1021/acsomega.1c02282
ACS Omega 2021, 6, 20341−20350

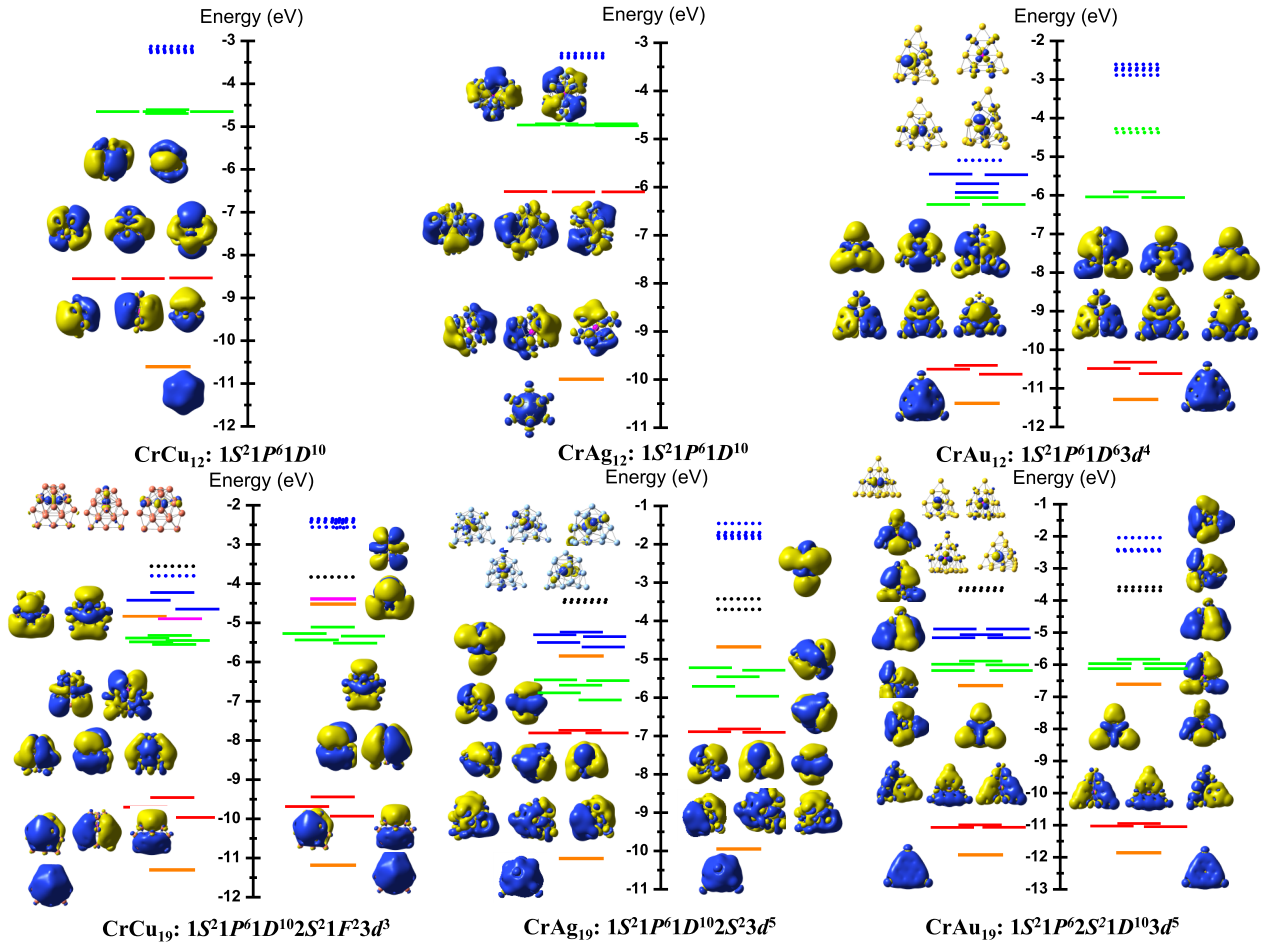

Figure 5. Molecular orbital diagrams for CrM_n (n = 12 and 19) with pictures of the delocalized orbitals and the localized 3d Cr orbitals. The orange, red, green, violet, and dark orange lines represent orbitals corresponding to the 1S, 1P, 1D, 1F, and 2S shells, respectively. The blue lines represent the localized 3d Cr orbitals. The filled lines stand for occupied orbitals while the dashed lines denote the unoccupied ones.

magnetic moment of 3 μ_B. Our calculations reveal that unlike in $CrCu_9$ and $CrAu_9$ clusters, there is a mixing between the dopant 3d electrons and the electrons in the silver in $CrAg_9$, providing a joint orbital of $1P_z^2/1D_\uparrow^2/3d^3/1D_\downarrow^2$. The formation of these overlap orbitals has a stabilizing effect on the bonding between silver and chromium and possibly enhances the stability of $CrAg_9$.

In the case of the icosahedral $CrCu_{12}$ and $CrAg_{12}$, all six valance electrons of the chromium are part of fully delocalized orbitals bound in a spherically symmetric potential well, resulting in the closed-shell structures of $1S^21P^61D^{10}$ and quenched magnetic moments. $CrCu_{12}$ and $CrAg_{12}$ have a large highest occupied molecular orbitals−lowest unoccupied molecular orbitals (HOMO−LUMO) gaps of 1.53 and 1.42 eV, respectively, which are responsible for their enhanced stability observed in Figure 2. Not only transition-metal-doped coinage clusters but the shell model also gives consistent interplay between the stability and electronic structure for doped Si, Sn, or Pb clusters.[43−49] To a certain extent, the magnetic suppression in $CrCu_{12}$ and $CrAg_{12}$ can be conceptually described by the Kondo model as in larger systems.[10] A similar story was reported for the doped silver clusters $CoAg_{10}^+$ and $FeAg_{10}$. The pronounced stability of $CoAg_{10}^+$ observed in photofragmentation experiments is also explained by the closed 18-electron singlet electronic shell structure.[18] The latter case is somewhat different since the suppressed magnetic moment of $FeAg_{10}$ is attributed to a spin-compensating electron cloud[19] rather than the formation of an 18-electron shell closure.

It is interesting to discuss the stability enhancement of closed-shell systems from the superatomic point of view. The literature has shown some specific clusters that behave like a single atom. This similarity, on the basis of the shell model theory,[2,3] has led to the conceptual development of a new class of clusters called superatoms.[50,51] Unlike bulk materials, atomic clusters have discrete energy levels. In the phenomenological shell model, delocalized electrons of all atoms are bound in a potential well formed by nuclei. It is analogous, because, in an atom, valence electrons move in the mean field created by the nucleus. The valence electrons fill cluster orbitals and the successive occupation of a shell/subshell leads to a stable species, characterized by a large HOMO−LUMO gap. The significant values of 1.53 and 1.42 eV found for $CrCu_{12}$ and $CrAg_{12}$ imply their particular high stability on the basis of the superatom concept.

It should be mentioned that the existing definition of superatoms can be extended to magnetic species. If a cluster obtains high stability through the closed electronic shells of diffused electrons while there are still localized orbitals having enough exchange splitting to cause a magnetic moment, it can be considered as a magnetic superatom.[13] A detailed analysis of the molecular orbitals allows us to understand the interplay between the geometric structure, electronic structure, and magnetic

https://doi.org/10.1021/acsomega.1c02282
ACS Omega 2021, 6, 20341−20350

superatomic features in $CrCu_{19}$, $CrAg_{19}$, and $CrAu_{19}$ clusters. Both $CrCu_{19}$ and $CrAg_{19}$ have unsymmetrical endohedral structures. $CrCu_{19}$ has an open-shell configuration of $1S^21P^61D^{10}2S^21F^23d^3$ with 22 valence electrons. The geometry of $CrCu_{19}$ allows the 1F orbitals to be pulled down in energy, leaving three localized 3d electrons in the spin majority channel, responding to a magnetic moment of 3 μ_B. The LUMO consists of two degenerate 3d chromium states, resulting in a small band gap (0.25 eV). The electronic configuration of $CrAg_{19}$ is $1S^21P^61D^{10}2S^23d^5$. Its LUMO is constructed from the cluster 1F orbitals while HOMO is characterized by five 3d chromium states, resulting in a band gap of 0.39 eV. Similar to the magic pyramid Au_{20}, the existence of closed electronic shells in compliance with the 20-electron rule has been observed for $CrAu_{19}$. The tetrahedral geometry of $CrAu_{19}$ allows 2S orbitals to strongly drop in energy, giving a fully occupied electron shell sequence of $1S^21P^62S^21D^{10}$. The atomic localized states 3d are half-filled with five unpaired electrons, causing a magnetic moment of 5 μ_B. Notably, $CrAu_{19}$ has the largest HOMO−LUMO gap of 0.78 eV, which means that this atom is the most stable, is least reactive, but has the highest spin compared to other n equal to 19 species, and can be assigned as a magnetic superatom.

CONCLUSIONS

In this article, we presented a systematic investigation on the electronic and geometric properties of $CrCu_n$, $CrAg_n$, and $CrAu_n$ clusters (n = 2−20) using the density functional theory calculations. For the geometric structure, our calculations show that the Cr dopant tends to occupy the most highly coordinated position. While the tetrahedron is still a basic framework for the growth process of $CrAu_n$ as well as their pure counterparts, doping a Cr dopant triggers a structural modification of $CrCu_n$ and $CrAg_n$ via the central icosahedral structure. For the electronic structure, the valence electrons in host noble atoms and transition-metal dopants are hybridized, forming two possible sets of orbitals: the localized and the delocalized ones. The itinerant electrons fill the cluster shells, whereas the localized orbitals cause the magnetic moment. $CrAg_9$, $CrCu_{12}$, $CrAg_{12}$, and $CrAu_{19}$ are found to be relatively stable compared with other species. The stability of these clusters is governed by not only their highly symmetric structures (except for $CrAg_9$) but also the enhancement in electronic stability by a full occupation of the delocalized electron shells. Molecular orbital analysis in combination with the shell model is carried out to understand the rigorous interaction between the geometric structure, electronic structure, and magnetic moment of the clusters. It is found that the shell structure and occupation level depend on whether the geometry of the cluster is two-dimensional or three-dimensional, spherical-like or tetrahedral, and so on. From the superatomic point of view, the $CrCu_{12}$ and $CrAg_{12}$ icosahedrons mimic a noble gas while the tetrahedral $CrAu_{19}$ can perform as a magnetic superatom. This study has revealed that substituting a noble host atom with a magnetic dopant causes subtle changes to the structure, bonding, stability, and magnetism of the clusters. Together with the existing knowledge on other impurities, for example, vanadium,[27] these results could contribute to a better understanding of the physics of magnetic materials in nonmagnetic metal clusters and could lead to rational designs of cluster-based nanostructured materials.

ASSOCIATED CONTENT

Supporting Information

The Supporting Information is available free of charge at https://pubs.acs.org/doi/10.1021/acsomega.1c02282.

Calculated geometries of ground-state structures and stable low-lying isomers of CrM_n (M = Cu, Ag, and Au) clusters with (n = 2−20); the molecular orbital (MO) diagrams of CrM_{2-20} (except for n = 6, 9, 12, and 19); and the Cartesian coordinates of the optimized clusters $CrCu_n$, $CrAg_n$, and $CrAu_n$ (PDF)

AUTHOR INFORMATION

Corresponding Authors

Nguyen Thi Mai − *Institute of Materials Science and Graduate University of Science and Technology, Vietnam Academy of Science and Technology, Hanoi 11307, Vietnam*; Email: maint@ims.vast.ac.vn

Ngo Thi Lan − *Institute of Materials Science and Graduate University of Science and Technology, Vietnam Academy of Science and Technology, Hanoi 11307, Vietnam; Department of Physics and Technology, Thai Nguyen University of Science, Thai Nguyen 250000, Vietnam*; Email: lan23101989@gmail.com

Ngo Tuan Cuong − *Center for Computational Science, Hanoi National University of Education, Hanoi 11310, Vietnam*; Email: cuongnt@hnue.edu.vn

Nguyen Minh Tam − *Computational Chemistry Research Group, Ton Duc Thang University, Ho Chi Minh City 72915, Vietnam; Faculty of Applied Sciences, Ton Duc Thang University, Ho Chi Minh City 72915, Vietnam*; Email: nguyenminhtam@tdtu.edu.vn

Son Tung Ngo − *Faculty of Applied Sciences and Laboratory of Theoretical and Computational Biophysics, Ton Duc Thang University, Ho Chi Minh City 72915, Vietnam*; orcid.org/0000-0003-1034-1768; Email: ngosontung@tdtu.edu.vn

Thu Thi Phung − *University of Science and Technology of Hanoi, Vietnam Academy of Science and Technology, Hanoi 11307, Vietnam*; Email: thuphungi2@gmail.com

Nguyen Van Dang − *Department of Physics and Technology, Thai Nguyen University of Science, Thai Nguyen 250000, Vietnam*; Email: dangnv@tnus.edu.vn

Nguyen Thanh Tung − *Institute of Materials Science and Graduate University of Science and Technology, Vietnam Academy of Science and Technology, Hanoi 11307, Vietnam*; orcid.org/0000-0003-0232-7261; Email: tungnt@ims.vast.ac.vn

Complete contact information is available at: https://pubs.acs.org/10.1021/acsomega.1c02282

Notes

The authors declare no competing financial interest.

ACKNOWLEDGMENTS

This research was supported by the Vietnam Ministry of Education and Training under grant number B2020-TNA-16 and the Institute of Materials Science, Vietnam Academy of Science and Technology under grant CS13/20-21.

REFERENCES

(1) Mathew, A.; Pradeep, T. Noble Metal Clusters: Applications in Energy, Environment, and Biology. *Part. Part. Syst. Charact.* **2014**, *31*, 1017−1053.

(2) de Heer, W. A. The Physics of Simple Metal Clusters: Experimental Aspects and Simple Models. *Rev. Mod. Phys.* **1993**, *65*, 611−676.
(3) Brack, M. The Physics of Simple Metal Clusters: Self-Consistent Jellium Model and Semiclassical Approaches. *Rev. Mod. Phys.* **1993**, *677*, 732.
(4) Muñoz-Castro, A.; King, R. B. Au_{10}^{2+} and $Au_6X_4^{2+}$ Clusters: Superatomic Molecules Bearing an SP^3-hybrid Au_6 Core. *Int. J. Quantum. Chem.* **2017**, *117*, No. e25331.
(5) Gam, F.; Arratia-Pérez, R.; Kahlal, S.; Saillard, J.-Y.; Muñoz-Castro, A. $[M_{16}Ni_{24}(CO)_{40}]^{4-}$: Coinage Metal Tetrahedral Superatoms as Useful Building Blocks Related to Pyramidal Au_{20} Clusters (M = Cu, Ag, Au). Electronic and Bonding Properties from Relativistic DFT Calculations. *J. Phys. Chem. C* **2018**, *122*, 4723−4730.
(6) Gam, F.; Arratia-Pérez, R.; Kahlal, S.; Saillard, J.-Y.; Muñoz-Castro, A. Potential to Stabilize 16-vertex Tetrahedral Coinage-metal Cluster Architectures Related to Au_{20}. *Phys. Chem. Chem. Phys.* **2019**, *21*, 8428−8433.
(7) Chen, Y.; Tang, Z.; He, C.; Sheng, Y. Density functional theory study of structural, Magnetic and Spectral Properties of the Cr_mFe_n ($m + n = 6$) and Cr_mFe_nCu ($m + n = 5$) Clusters. *Mater. Express* **2019**, *9*, 570−577.
(8) Song, W.; Fu, Z.; Wang, J.-L.; Zhang, W. Structural, Electronic and Magnetic Properties of NM-doped Ni Clusters (NM = Cu, Ag, Au). *J. Mol. Struct.* **2019**, *1197*, 147−153.
(9) Friedel, J. Metallic Alloys. *Nuovo Cimento* **1958**, *7*, 287−311.
(10) Kondo, J. Resistance Minimum in Dilute Magnetic Alloys. *Prog. Theor. Phys.* **1964**, *32*, 37−49.
(11) Manoharan, H. C.; Lutz, C. P.; Eigler, D. M. Quantum Mirages Formed by Coherent Projection of Electronic Structure. *Nature* **2000**, *403*, 512−515.
(12) Nygård, J.; Cobden, D. H.; Lindehof, P. E. Kondo Physics in Carbon Nanotubes. *Nature* **2000**, *408*, 342−346.
(13) Reveles, J. U.; Clayborne, P. A.; Reber, A. C.; Khanna, S. N.; Pradhan, K.; Sen, P.; Pederson, M. R. Designer Magnetic Superatoms. *Nat. Chem.* **2009**, *1*, 310−315.
(14) Medel, V. M.; Reber, A. C.; Chauhan, V.; Sen, P.; Köster, A. M.; Calaminici, P.; Khanna, S. N. Nature of Valence Transition and Spin Moment in Ag_nV^+ Clusters. *J. Am. Chem. Soc.* **2014**, *136*, 8229−8236.
(15) Hirsch, K.; Zamudio-Bayer, V.; Langenberg, A.; Niemeyer, M.; Langbehn, B.; Moller, T.; Terasaki, A.; Issendorff, Bv.; Lau, J. T. Magnetic Moments of Chromium-Doped Gold Clusters: The Anderson Impurity Model in Finite Systems. *Phys. Rev. Lett.* **2015**, *114*, No. 087202.
(16) Tam, N. M.; Pham, H. T.; Cuong, N. T.; Tung, N. T. $Au_{19}M$ (M = Cr, Mn, and Fe) as Magnetic Copies of the Golden Pyramid. *Sci. Rep.* **2017**, *7*, No. 16086.
(17) Tam, N. M.; Mai, N. T.; Pham, H. T.; Cuong, N. T.; Tung, N. T. Ultimate Manipulation of Magnetic Moments in the Golden Tetrahedron Au_{20} with a Substitutional 3*d* Impurity. *J. Phys. Chem. C* **2018**, *122*, 16256−16264.
(18) Janssens, E.; Neukermans, S.; Nguyen, H. M. T.; Nguyen, M. T.; Lievens, P. Quenching of the Magnetic Moment of a Transition Metal Dopant in Silver Clusters. *Phys. Rev. Lett.* **2005**, *94*, No. 113401.
(19) Dong, R.; Chen, X.; Zhao, H.; Wang, X.; Shu, H.; Ding, Z.; Wei, L. Structural, Electronic and Magnetic Properties of Ag_nFe Clusters ($n \leqslant 15$): Local Magnetic Moment Interacting with Delocalized Electrons. *J. Phys. B: At., Mol. Opt. Phys.* **2011**, *44*, No. 035102.
(20) Höltzl, T.; Veldeman, N.; Haeck, J. D.; Veszprémi, T.; Lievens, P.; Nguyen, M. T. Growth Mechanism and Chemical Bonding in Scandium-Doped Copper Clusters: Experimental and Theoretical Study in Concert. *Chem. - Eur. J.* **2009**, *15*, 3970−3982.
(21) Höltzl, T.; Janssens, E.; Veldeman, N.; Veszprémi, T.; Lievens, P.; Nguyen, M. T. The Cu_7Sc Cluster is a Stable σ-Aromatic Seven-Membered Ring. *Chem. Phys. Chem.* **2008**, *9*, 833−838.
(22) Veldeman, N.; Höltzl, T.; Neukermans, S.; Veszprémi, T.; Nguyen, M. T.; Lievens, P. Experimental Observation and Computational Identification of $Sc@Cu_{16}^+$, a Stable Dopant-Encapsulated Copper Cage. *Phys. Rev. A* **2007**, *76*, No. 011201.
(23) Zhang, M.; Zhang, H.; Zhao, L.; Li, Y.; Luo, Y. Low-Energy Isomer Identification, Structural Evolution, and Magnetic Properties in Manganese-Doped Gold Clusters $MnAu_n$ (n = 1-16). *J. Phys. Chem. A* **2012**, *116*, 1493−1502.
(24) Boulbazine, M.; Boudjahem, A.-G. Stability, Electronic and Magnetic Properties of Mn-doped Copper Clusters: A Meta-GGA Functional Investigation. *J. Cluster Sci.* **2019**, *30*, 31−44.
(25) Die, D.; Zheng, B.-X.; Zhao, L.-Q.; Zhu, Q.-W.; Zhao, Z.-Q. Insights into the Structural, Electronic and Magnetic Properties of V-doped Copper Clusters: Comparison with Pure Copper Clusters. *Sci. Rep.* **2016**, *6*, No. 31978.
(26) Xiong, R.; Die, D.; Xiao, L.; Xu, Y.-G.; Shen, X.-Y. Probing the Structural, Electronic, and Magnetic Properties of Ag_nV (n = 1-12) Clusters. *Nanoscale Res. Lett.* **2017**, *12*, No. 625.
(27) Blades, W. H.; Reber, A. C.; Khanna, S. N.; López-Sosa, L.; Calaminici, P.; Köster, A. M. Evolution of the Spin Magnetic Moments and Atomic Valence of Vanadium in VCu_x^+, VAg_x^+, and VAu_x^+ Clusters (x = 3−14). *J. Phys. Chem. A* **2017**, *121*, 2990−2999.
(28) Pham, H. T.; Cuong, N. T.; Tam, N. M.; Tung, N. T. A systematical investigation on $CrCu_n$ clusters with n = 9-12: Noble gas and tunable magnetic property. *J. Phys. Chem. A* **2016**, *120*, 7335−7343.
(29) Frisch, M. J.; Schlegel, H. B.; Scuseria, G. E.; Robb, M. A.; Cheeseman, J. R.; Montgomery, J. A.; Vreven, T.; Kudin, K. N.; Burant, J. C.; Millam, J. et al. *Gaussian 09*, revision: D.01; Gaussian, Inc.: Wallingford, CT, 2009.
(30) Tai, T. B.; Nguyen, M. T. A Stochastic Search for the Structures of Small Germanium Clusters and Their Anions: Enhanced Stability by Spherical Aromaticity of the Ge_{10} and Ge_{12}^{2-} Systems. *J. Chem. Theory Comput.* **2011**, *7*, 1119−1130.
(31) Supplementary Material.
(32) Dong, D.; Xiao-Yu, K.; Jian-Jun, G.; Ben-Xia, Z. Geometries, stabilities, and magnetic properties of $Cr@Au_n$ (n = 1-8) clusters: Density functional theory study. *Phys. A* **2010**, *389*, 5216−5222.
(33) Ben-Xia, Z.; Dong, D.; Ling, W.; Ji-Xian, Y. Density Functional Study on the Structural, Electronic, and Magnetic Properties of 3*d* Transition-Metal-Doped Au_5 Clusters. *J. Phys. Chem. A* **2014**, *118*, 4005−4012.
(34) Itoh, M.; Kumar, V.; Adschiri, T.; Kawazoe, Y. Comprehensive Study of Sodium, Copper, and Silver Clusters over a Wide Range of Sizes $2 \leqslant N \leqslant 75$. *J. Chem. Phys.* **2009**, *131*, No. 174510.
(35) Chen, M.; Dyer, J. E.; Li, K.; Dixon, D. A. Prediction of Structures and Atomization Energies of Small Silver Clusters, $(Ag)_n$, $n < 100$. *J. Phys. Chem. A* **2013**, *117*, 8298−8313.
(36) Xiao, L.; Tollberg, B.; Hu, X.; Wang, L. Structural study of gold clusters. *J. Chem. Phys.* **2006**, *124*, No. 114309.
(37) Harb, M.; Rabilloud, F.; Simon, D.; Rydlo, A.; Lecoultre, S.; Conus, F.; Rodrigues, V.; Felix, C. Optical absorption of small silver clusters: Ag_n, (n = 4-22). *J. Chem. Phys.* **2008**, *129*, No. 194108.
(38) Jiang, M.; Zeng, Q.; Zhang, T.; Yang, M. Icosahedral to Double-Icosahedral Shape Transition of Copper Clusters. *J. Chem. Phys.* **2012**, *136*, No. 104501.
(39) Tafoughalt, M. A.; Samah, M. Structural properties and relative stability of silver-doped gold clusters $AgAu_{n-1}$ (n = 3-13): Density functional calculations. *Comput. Theor. Chem.* **2014**, *1033*, 23−30.
(40) Zhu, B.; Die, D.; Li, R. C.; Lan, H.; Zheng, B. X.; Li, Z. Q. Insights into the structural, electronic and magnetic properties of Ni-doped gold clusters: Comparison with pure gold clusters. *J. Alloy. Compd.* **2017**, *696*, No. 402e412.
(41) Hansen, K. *Statistical Physics of Nanoparticles in the Gas Phase*; Springer: Dordrecht Heidelberg, New York, London, 2013.
(42) Bhattacharyya, S.; Nguyen, T. T.; De Haeck, J.; Hansen, K.; Lievens, P.; Janssens, E. Mass-selected Photodissociation Studies of $AlPb_n^+$ Clusters (n = 7-16): Evidence for the Extraordinary Stability of $AlPb_{10}^+$ and $AlPb_{12}^+$. *Phys. Rev. B* **2013**, *87*, No. 054103.
(43) Goicoechea, J. M.; McGrady, J. E. On the Structural Landscape in Endohedral Silicon and Germanium Clusters, $M@Si_{12}$ and $M@Ge_{12}$. *Dalton Trans.* **2015**, *44*, 6755−6766.
(44) Abreu, M. B.; Reber, A. C.; Khanna, S. N. Does the 18-Electron Rule Apply to $CrSi_{12}$? *J. Phys. Chem. Lett.* **2014**, *5*, 3492−3496.

https://doi.org/10.1021/acsomega.1c02282
ACS Omega 2021, 6, 20341−20350

(45) King, R. B.; Silaghi-Dumitrescu, I.; Uta, M. M. The Unique Palladium-Centered Pentagonal Antiprismatic Cationic Bismuth Cluster: A Comparison of Related Metal-Centered 10-Vertex Pnictogen Cluster Structures by Density Functional Theory. *Inorg. Chem.* **2009**, *48*, 8508−8514.
(46) Zhou, B.; Kramer, T.; Thompson, A. L.; McGrady, J. E.; Goicoechea, J. M. A Highly Distorted Open-Shell Endohedral Zintl Cluster: $[Mn@Pb_{12}]^{3-}$. *Inorg. Chem.* **2011**, *50*, 8028−8037.
(47) Huang, X.; Xu, H.-G.; Lu, S.; Su, Y.; King, R. B.; Zhao, J.; Zheng, W. Discovery of a Silicon-Based Ferrimagnetic Wheel Structure in $V_xSi_{12}^-$ (x = 1-3) Clusters: Photoelectron Spectroscopy and Density Functional Theory Investigation. *Nanoscale* **2014**, *6*, 14617−14621.
(48) Esenturk, E. N.; Fettinger, J.; Eichhorn, B. The Pb_{12}^{2-} and Pb_{10}^{2-} Zintl Ions and the $M@Pb_{12}^{2-}$ and $M@Pb_{10}^{2-}$ Cluster Series Where M=Ni, Pd, Pt. *J. Am. Chem. Soc.* **2006**, *128*, 9178−9186.
(49) Uţă, M. M.; Cioloboc, D.; King, R. B. Iron-Centered Ten-Vertex Germanium Clusters: The Ubiquity of Low Energy Pentagonal Prismatic Structures with Various Skeletal Electron Counts. *J. Phys. Chem. A* **2012**, *116*, 9197−9204.
(50) Khanna, S. N.; Jena, P. Atomic Clusters: Building Blocks For a Class of Solids. *Phys. Rev. B* **1995**, *51*, 13705−13716.
(51) Medel, V. M.; Reber, A. C.; Chauhan, V.; Sen, P.; Köster, A. M.; Calaminici, P.; Khanna, S. N. Nature of Valence Transition and Spin Moment in Ag_nV^+ Clusters. *J. Am. Chem. Soc.* **2014**, *136*, 8229−8236.

https://doi.org/10.1021/acsomega.1c02282
ACS Omega 2021, 6, 20341−20350